Resonant Parallel Shear Instability in the Stably Stratified Planetary Boundary Layer

P. A. DAVIS AND W. R. PELTIER

Department of Physics, University of Toronto, Toronto, Ontario, Canada M5S 1A7

(Manuscript received 5 January 1976, in revised form 29 March 1976)

ABSTRACT

We consider a compressible, inviscid, stratified parallel shear flow, bounded below by a rigid wall and above by a half-space of constant wind speed and temperature. Linear stability analysis shows that this flow is unstable to a family of modes, one of which is the well-known Kelvin-Helmholtz disturbance. The remaining modes, here called resonant modes, undergo little attention in the region below the shear layer, and their parameters and structure are strongly influenced by the presence of the ground.

The stability curves for both types of modes are investigated as functions of the parameters of the background state. For most combinations of parameters, the resonant modes are trapped between their critical level and the ground. However, for nearly isentropic shear layers, the neutral resonant modes become free to propagate in the upper half-space. Under such conditions, the growing solutions are no longer contiguous to the neutral curves. The growth rates of the Kelvin-Helmholtz modes are found to be larger than those of the resonant modes for all combinations of the background parameters. The evolution of instabilities in a real shear layer is discussed in the light of this result. The eigenfunction structure of the resonant modes suggests an explanation for the multiple thin scattering layers often recorded by radars observing the stable boundary layer.

1. Introduction

There is a long history of investigations into the stability of a parallel shear flow. The study began with Helmholtz, who determined the stability criterion for an unbounded atmosphere with step discontinuities in wind speed and density. Kelvin was able to show that the resulting nonlinear disturbance developed a braided, or cat's-eye, pattern. Subsequent analyses dealt with continuous wind speed and density profiles (Drazin, 1958; Hazel, 1972) and more realistic boundary conditions (Jones, 1968). But in all of these models certain features of the fastest growing instability were common: a phase speed equal to the speed of the background wind at the center of the shear layer, a horizontal wavelength proportional to the depth of the shear layer, and an amplitude which decayed rapidly away from the region of shear. In this paper, any mode of instability displaying these characteristics will be called a Kevin-Helmholtz, or K-H instability, although this term has often been reserved for the discontinuous velocity profile case.

The K-H disturbance is able to smooth the original shear layer by extracting energy from the mean flow, amplifiying in time locally, and breaking to dissipate the energy in turbulence. However, if the stratification remains stable away from the shear zone, the possibility exists that the shear energy can be used instead to generate an internal wave, which deposits the energy at great distances from the shear layer at the time of its re-absorption by the mean flow. Lindzen (1974) has examined the stability of a discontinuous velocity profile in an unbounded, isothermal atmosphere and found that although short-wavelength perturbations had the characteristics of K-H disturbances, long-wavelength perturbations manifested themselves as neutral internal gravity waves. The same behavior was indicated in the work of Jones (1968) for a piecewise linear velocity profile in an unbounded, isothermal atmosphere. In addition, recent analyses have shown that instabilities in Ekman layer flows (Kaylor and Faller, 1972), in stable boundary layers subject to diurnal variations in stability (Orlanski, 1973), and in large-scale barotropic shear flows (Dickinson and Clare, 1973) can all be interpreted as resonances with internal waves.

The ubiquitous presence of K-H disturbances of various scales in the stable boundary layer (Emmanual *et al.*, 1972; Browning *et al.*, 1973) implies that unstable parallel shear flows are common here. If such flows are also capable of internal wave generation, they could account for some of the many wave events observed in the boundary layer (Gossard *et al.*, 1970; Metcalf, 1975). In particular, the thin, wavy, coherent multiple layers, regularly spaced in the vertical, that are commonly observed by acoustic and FM-CW radars, suggest an explanation in terms of linear theory. A

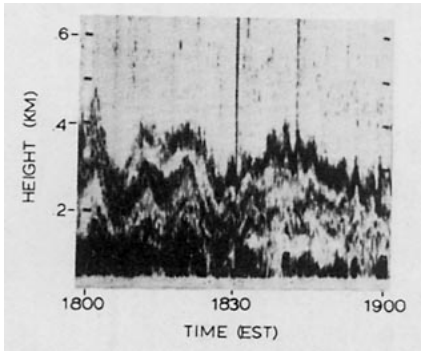

FIG. 1. Acoustic sounder record for 3 July 1974 at Toronto. Between 1800 and 1900 EST, three wavy, coherent scattering layers, periodically spaced in the vertical, are found below 400 m. The layers are actually considerably thinner than they appear to be on the record since the vertical resolution of the sounder is about 20 m.

typical example of a multiple layer event is shown in Fig. 1, recorded with the acoustic sounder operating in urban Toronto, and described by Bennett (1975). Gossard *et al.* (1971) have given an explanation of such layers in terms of untrapped gravity waves propagating nearly vertically as they enter a region of strong static stability. Such an explanation is somewhat artificial in that it makes use of waves generated far from the regions of the multiple layers themselves. In addition, since no temperature or wind profiles are available for periods during which the multiple layers have been observed, it is not obvious that the conditions required for the achievement and maintenance of the vertical propagation of these waves are present.

The aim or the present paper is to analyze the complete stability problem of a stratified parallel shear flow in a boundary layer setting. We will show that such a flow is unstable to disturbances with the character of internal gravity waves and that these disturbances could be responsible for the formation of the observed thin multiple layers.

2. Theory

a. Review of previous results

Summarized below are some pertinent theorems on the nature of the instabilities of a general parallel shear flow in an atmosphere that is stratified, inviscid, incompressible and unbounded.

I. A necessary, though not sufficient, condition for instability is that the Richardson number Ri drop below 0.25 somewhere in the flow (Miles, 1961; Howard, 1961). The Richardson number is a measure of the relative importance of the stabilizing influence of the stratification to destabilizing inertial effects, and is defined by

$$\mathrm{Ri}=\frac{N^2}{(\partial V/\partial z)^2}=\frac{g}{\theta}\frac{\partial\theta/\partial z}{(\partial V/\partial z)^2},$$

where V is the speed of the flow, θ the potential temperature, g the gravitational acceleration and N the Brunt-Väisälä frequency.

II. The complex phase speed c of any unstable mode must lie within the semi-circle in the upper c plane which has the given range of background wind speeds for diameter (Howard, 1961). This theorem implies that the real phase speed of an unstable mode must match the speed of the background wind somewhere in the flow. At such a level, called the critical level, the Doppler-shifted frequency of the perturbation becomes zero.

III. The growth rate of any unstable mode must be less than a value which depends upon the parameters of the background flow (Howard, 1961).

IV. Unstable perturbations must be bounded by a neutral curve composed of singular neutral modes (Miles, 1961). A neutral mode is a solution to the stability equation which neither grows nor decays in time. The term "singular" refers to a mode which has a critical level somewhere in the flow.

V. The existence of a neutral curve implies the existence of at least one contiguous growing solution in the Richardson number-wavenumber plane (Miles, 1963).

Theorems I and III have been extended to compressible flows with a single rigid boundary by Chimonas (1970). Theorem II has been extended to compressible flows by Eckert (1963), who was able to place more restrictive but less specific limitations on c.

b. The model atmosphere

Since we wish to look for wavelike instabilities in a boundary layer setting, the atmospheric model we assume is bounded below by a rigid wall and above by a radiation condition. Although the model is capable of simulating the wide variety of wind and temperature profiles observed in the boundary layer, in this paper we shall discuss only hyperbolic tangent profiles in order to make the presentation more systematic. The profiles used in the model have the form

$$U=U_0\{1+\tanh[(z-z_i)/h]\}, \tag{1}$$

$$T=T_0+\alpha\beta\tanh[(z-z_i)/(\beta h)]. \tag{2}$$

Here z_i is the height above the ground of the inflection points in both profiles, and h is a measure of the depth over which the wind and temperature gradients are large. For comparison with other models the depth of the shear layer will be taken as $\Delta z=2h$. In Eq. (2) α is a measure of the change in temperature across the inversion, and can be either positive or negative, while β is essentially the ratio of the distance over which the temperature gradients are large to the distance over which the shear is large. A value of $\beta>1$ implies a narrow shear zone embedded in a broad temperature inversion, while $\beta<1$ implies a broad shear zone con-

taining a narrow inversion. The values of U_0 and T_0 were fixed at 2.4 m s^{-1} and 271 K, respectively. Asymptotic values of U above and below the shear layer respectively are $2U_0$ and 0, and with $T_0+\alpha\beta$ and $T_0-\alpha\beta$ the corresponding temperatures.

Because U and T vary continuously with height, there is no Richardson number that is applicable to the entire flow. The value to be used in the following discussions will be the Richardson number at the inflection point height, i.e.,

$$\mathrm{R}=\frac{g}{T_0}\frac{(\alpha/h+\Gamma)}{(U_0/h)^2},$$

where Γ is the negative of the adiabatic lapse rate. Note that R varies with α and h, but is independent of β.

The model atmosphere is assumed to be non-rotating, inviscid and non-heat-conducting. The first of these simplifications means that we are restricting our attention to the acoustic-gravity wave régime. The effects of viscosity and thermal interchange on the linear results will be discussed in Section 4.

The model was allowed to be compressible, and in this respect it differs from almost all other models in the literature. The effects of compressibility are expected to be small, but perhaps significant when dealing with the short length and time scales for shear layers located very close to the ground. In addition, we wish to apply our results to actual observations, and interpretations, particularly in terms of the Brunt-Väisälä frequency, would be inconvenient if an incompressible framework were adopted. Finally, the effects of compressibility determine the exact frequency at which the character of the instability changes from evanescent to propagating in the isothermal, constant wind layers above and below the shear zone (Jones, 1968).

Since we are dealing with a parallel flow, we choose the x axis of our coordinate system to lie along the direction of flow. The z axis is directed anti-parallel to $\mathbf{g}$, with origin at the rigid lower boundary.

c. Derivation of the stability equation

The equations of motion, continuity and adiabatic state for the model atmosphere described above are, respectively,

$$\frac{D\mathbf{U}^*}{Dt}+\frac{\nabla p^*}{\rho^*}+\mathbf{g}=0, \tag{3}$$

$$\frac{D\rho^*}{Dt}+\rho^*\nabla\cdot\mathbf{U}^*=0, \tag{4}$$

$$\frac{Dp^*}{Dt}-\frac{\gamma p^*}{\rho^*}\frac{D\rho^*}{Dt}=0, \tag{5}$$

where $\mathbf{U}^*=(u^*, w^*)$ is the total wind vector, p^* and ρ^* are the total pressure and density, and γ is the ratio of specific heats. D/Dt is the substantive derivative

$$D/Dt=\partial/\partial t+\mathbf{U}^*\cdot\nabla.$$

We wish to examine the response of this system to a general perturbation, or equivalently, the response to each Fourier component of a general perturbation in turn. Each total variable is therefore understood to consist of a mean (capitalized) and perturbation (primed) part. The mean variables will be functions of z only, according to our model of the mean state. The perturbations may be considered two-dimensional on the basis of Yih's (1955) remark that three-dimensional disturbances of the same wavelength are generally more stable. The perturbation will then have the form of a wave periodic in the x direction. For example,

$$w'(x, z, t)=w(z)\exp[i(\omega t-kx)], \tag{6}$$

where k is the horizontal wavenumber of the perturbation and is assumed real, so that the wave propagates freely in the horizontal; $\omega=\omega_r+i\omega_i$ is the disturbance frequency, and is assumed to be complex in order to admit perturbations, with negative ω_i and ω_r positive, that will grow in time; and $w(z)$ is the height-dependent part of $w'(x, z, t)$, and is to be determined.

We proceed by substituting these expressions for the total variables into Eqs. (3)–(5) and linearizing the resulting set by neglecting terms of order greater than 1 in perturbation quantities. This linearized set can be reduced to a single equation in any one of the perturbation quantities. We choose to work with the perturbation vertical velocity for ease in applying the boundary conditions. We obtain (Chimonas, 1970)

$$\left[\frac{r\sigma^2 q'}{k^2-(\sigma/C)^2}\right]'+r(N^2-\sigma^2)q=0, \tag{7}$$

where

$$\left.\begin{aligned} q&=\frac{w(z)}{i\sigma}\exp\left(-g\int^z C^{-2}(y)dy\right)\\ r&=\rho_0(z)\exp\left(2g\int^z C^{-2}(y)dy\right)\end{aligned}\right\}.$$

Eq. (7) is the required stability equation: a prime here indicates differentiation with respect to z; $\sigma=\omega-kU$ is the Doppler-shifted frequency of the perturbation; $\rho_0(z)$ is the background density distribution; and $C^2=\gamma gH$ is the square of the background speed of sound, where H is the atmospheric scale height.

Eq. (7) is subject to the boundary conditions (i) $w=0$ at the ground, and (ii) the vertical energy flux above the shear layer must be outgoing, and the energy density at infinity bounded. The first condition is easily accommodated, but the second requires careful consideration. High above the shear layer the wind speed and temperature given by (1) and (2) are

essentially constant, and (7) reduces to

$$w''-\frac{w'}{H}+\left(\frac{\sigma^2}{C^2}+\frac{k^2\omega_g^2}{\sigma^2}-k^2\right)w=0, \tag{8}$$

where $\omega_g^2=(\gamma-1)g^2/C^2$ is the Brunt-Väisälä frequency for an isothermal atmosphere. The transformation $w=\phi e^{z/2H}$ puts (8) into canonical form

$$\phi''+\left(\frac{\sigma^2}{C^2}+\frac{k^2\omega_g^2}{\sigma^2}-k^2-\frac{\omega_a^2}{C^2}\right)\phi=0,$$

or

$$\phi''+l^2\phi=0$$

since we recognize

$$l^2=\frac{\sigma^2}{C^2}+\frac{k^2\omega_g^2}{\sigma^2}-k^2-\frac{\omega_a^2}{C^2} \tag{9}$$

as the dispersion equation for acoustic gravity waves in an isothermal, constant wind atmosphere (Hines, 1960). The parameter l is simply the vertical wavenumber of the wave under such circumstances, and $\omega_a=\gamma g/(2C)$ is the acoustic cutoff frequency. Therefore, the solution to (7) in the upper half-space is proportional to

$$w=e^{z/2H}e^{-ilz}=e^{(l_i+\frac{1}{2}H)z}e^{-il_rz}. \tag{10}$$

This equation in fact represents two solutions depending upon the sign of l_r; this sign must be chosen so that (10) represents a wave with upward energy flux. Now in an isothermal atmosphere at rest, upward energy propagation in a gravity wave implies the downward propagation of phase (Hines, 1960). But if at some level a background wind U_0 exists, and is greater than the horizontal phase speed ω_r/k of the wave, upward energy propagation will imply upward propagation of phase to an observer fixed on the ground. But this must always be the case for unstable modes if U_0 is taken to be the wind speed in the upper half-space, since $U_0>\omega_r/k$ is just Miles' (1961) condition that there exist a critical level for all unstable modes somewhere in the flow. Thus, l_r in (10) must always be positive. In addition, l_i must always be negative in order that the energy density of the perturbation at infinity be finite.

If the shear layer with its associated inversion is thin and located far from the wall, there will exist an isothermal, wind-free layer between the bottom of the shear zone and the ground. In this layer the solutions to (7) will again be of the form of (10), but now both upgoing and downgoing waves must be allowed.

We note for future reference that the real and imaginary parts of (9) are

$$l_r^2-l_i^2=k^2[\omega_g^2(\sigma_r^2-\sigma_i^2)/(\sigma_r^2+\sigma_i^2)^2-1]+(\sigma_r^2-\sigma_i^2-\omega_a^2)/C^2, \tag{11}$$

$$l_rl_i=\sigma_r\sigma_i\left[\frac{1}{C^2}-k^2\omega_g^2/(\sigma_r^2+\sigma_i^2)^2\right]. \tag{12}$$

d. Method of solution for growing modes

The stability equation (7) and the two boundary conditions form an eigenvalue problem, in that solutions exist only for certain values of the wave parameters ω_r, ω_i and k. These eigenvalues were determined in the following way. A particular set of wave parameters was chosen, essentially arbitrarily, although the choice was restricted somewhat by theorems II and III above, and by the desire for physically realistic solutions. The corresponding values of w_r and w_i in the upper half-space were calculated from (10), (11) and (12), and (7) was then integrated to the ground using a standard fourth-order Runge-Kutta routine. A table of solutions was built up by repeated application of this procedure. Interpolation in this table revealed which combinations of ω_r, ω_i and k, if any, led to simultaneous zero values of both w_r and w_i at the ground. Such combinations determine an eigenvalue set since these values led to the satisfaction of the lower boundary condition.

e. Method of solution for neutral modes

A straightforward integration of the stability equation is not possible in the case of neutral modes, since at the critical level for such modes the term $(\sigma_r^2+\sigma_i^2)$ must be zero, and some of the coefficients in (7) become infinite. It is possible to avoid this difficulty by using the method of Frobenius to construct an analytic solution to (7) in the vicinity of the critical level.

The analysis follows closely the work of Miles (1961) and Booker and Bretherton (1967). We assume that the solution to the stability equation is expressible in series form

$$w=\sum_{j=0}^{\infty}a_j(z-z_c-ic_i/U_c')^{m+j}\equiv\sum_{j=0}^{\infty}a_j\xi^{m+j}. \tag{13}$$

Here subscript c implies evaluation at the critical level; c_i is the imaginary phase speed of the perturbation, and although assumed arbitrarily small, must be carried through at this point in order to determine the behavior of ξ as the solution crosses the critical level.

Eq. (13) is now substituted into (7) and coefficients of successive powers of ξ collected. The coefficients of the lowest power in ξ lead to the indicial equation

$$m=\tfrac{1}{2}\pm\nu, \tag{14}$$

where $\nu=(\frac{1}{4}-\mathrm{R}_c)^{\frac{1}{2}}$ and is assumed for the moment to be real. The equation of the next highest power in ξ gives

$$\frac{a_1}{a_0}=\frac{1}{1+2\nu}\left[\frac{u_c''}{u_c'}(1-\mathrm{R}_c)-\mathrm{R}_c'+\frac{2}{\gamma H_c}+(-\tfrac{1}{2}\pm\nu)\left(\frac{1+H_c'}{H_c}\right)\right]\equiv A_{\pm}.$$

Therefore, the Frobenius solution to the stability equation near the critical level is, to second order,

$$w=a_{01}(\xi^{\frac{1}{2}+\nu}+A_+\xi^{\frac{3}{2}+\nu})+a_{02}(\xi^{\frac{1}{2}-\nu}+A_-\xi^{\frac{3}{2}-\nu}). \quad (15)$$

It was found in practice that the second-order terms were necessary to give solutions to better than 1%.

It remains to determine the behavior of ξ as the solution crosses the critical level. Now c_i is negative for growing solutions, so

$$\arg(\xi)=\tan^{-1}\{-c_i/[U_c'(z-z_c)]\}$$

varies from 0 to π as z varies from plus to minus infinity. Thus, $\xi=|\xi|$ above the critical level and $\xi=|\xi|e^{i\pi}$ below the critical level.

If it happens that $R_c>\frac{1}{4}$, the indicial equation becomes

$$m=\tfrac{1}{2}\pm i\mu,$$

where $\mu=(R_c-\frac{1}{4})^{\frac{1}{2}}$ and is real. All of the above theory continues to hold with ν replaced by $i\mu$.

The Frobenius solution (15) is applied as follows. The stability equation (7) is integrated as usual to a point just above the critical level. The solutions at this point are used to evaluate the coefficients a_{01} and a_{02} in (15). Once these are known, (15) is used to predict the values of w_r and w_i just below the critical level, where the numerical solution is resumed.

Except for these details near the critical level, the search for eigenvalues corresponding to neutral solutions proceeds in much the same way as the search for those corresponding to unstable solutions. The process is simplified a bit by the knowledge that ω_i is zero for neutral modes, so that the search for eigenvalues takes place in a table of solutions which are functions of ω_r and k only.

3. Results

The stability of the model will be discussed in terms of four background parameters: 1) z_i/h, the nondimensional distance of the shear layer above the ground; 2) β, the ratio of the scale of temperature variations to the scale of wind variations; 3) R_h, the Richardson number at the inflection-point height, as a function of the shear depth h, with α fixed; 4) R_α, the Richardson number at the inflection point height, as a function of stability α, with h fixed. Only one parameter will be varied at a time. When h, α and β are not varied explicitly, it is to be understood that they have values of 20 m, 0.8 K and 1, respectively. These values lead to profiles of wind speed and temperature that are commonly observed in the boundary layer (Emmanuel *et al.*, 1972), and to R=0.125, for which instabilities are possible.

Analysis has revealed that, depending upon the values of the background parameters, there may exist three distinct types of instability, which are distinguished from one another by their behavior far from the region of shear. These three modes of instability will be discussed in turn.

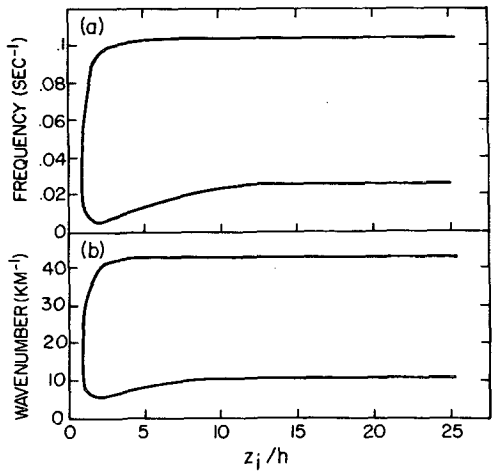

FIG. 2. Frequency (a) and wavenumber (b) of the neutral K-H mode as a function of z_i/h: $h=20$ m, $\alpha=0.8$ K, $\beta=1$.

a. Kelvin-Helmholtz modes

One member of this set of instabilities can be immediately identified as a K-H disturbance through its characteristic horizontal phase speed and wavelength, and its rapid attenuation away from the shear zone. Fig. 2 illustrates the dependence of the neutral K-H eigenvalues upon the distance of the shear layer from the wall. In this diagram, h is fixed while z_i is allowed to vary. Above a certain value of z_i/h, which is approximately 15 for the lower branch and 5 for the upper, the effect of the wall is negligible. This is due to the strong attenuation of these modes as a function of distance from the critical level. The modes comprising the upper branch suffer greater attenuation than do the modes comprising the lower branch, and so begin to feel the effects of the ground at smaller values of z_i/h. The ultimate effect of the wall is to completely stabilize the flow, as no instabilities are found for $z_i/h<0.9$.

Hazel (1972) has shown that a shear flow between two rigid boundaries is also stabilized when the boundaries begin to encroach upon the shear. He found that the stabilization occurred at $z_i/h=1.5$. The value found in this study is slightly lower, and reflects the decreased influence of a single boundary.

Fig. 2b indicates that there are two physical scales which complete to determine the horizontal wavelength of the perturbation. Consider the behavior of the lower branch of this curve. Far from the wall, the scale of the shear zone Δz is the only important scale, and k is independent of z_i/h. However, as z_i/h drops below 15 and the instability begins to feel the ground, the distance z_i of the shear zone from the wall enters as a second, and larger scale. At first the influence of this scale is weak, but as z_i/h decreases the influence of the wall becomes more pronounced and the z_i scale more

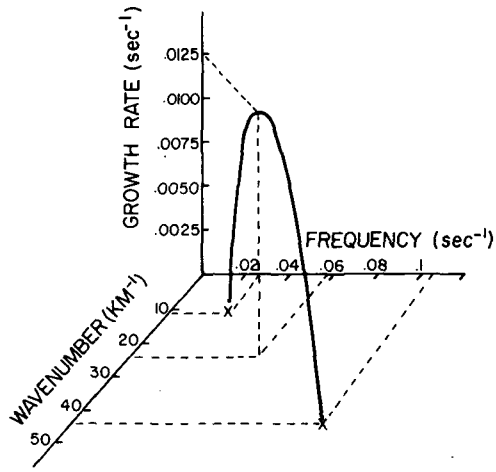

FIG. 3. Locus of unstable K-H eigenvalues in (ω_r, ω_i, k) parameter space at $z_i/h=15$; X's mark the location of the two associated neutral solutions: $h=20$ m, $\alpha=0.8$ K, $\beta=1$.

important. Thus, although z_i decreases as the shear layer approaches the ground, the new scale causes the wavelength to increase. This behavior continues until the ground begins to interfere with the shear layer itself at about $z_i/h=2$. At this point Δz becomes larger than z_i, and further decreases in z_i, which is now the dominant scale, lead to decreases in wavelength.

For any value of z_i/h in Fig. 2, the two neutral solutions are bounds for growing modes. The locus of unstable eigenvalues in (ω_r, ω_i, k) parameter space is shown in Fig. 3 for $z_i/h=15$. This figure illustrates the limited range of wavelengths to which the flow is unstable. The variation in the growth rate of the fastest growing modes with z_i/h is shown in Fig. 4. The stabilizing influence of the wall is apparent as growth rates decrease with decreasing z_i/h. The growth rate becomes zero at $z_i/h=0.9$, or at exactly the minimum distance for which neutral solutions exist.

Far from the wall the fastest growing modes show the characteristics expected of a K-H instability. The horizontal phase speed is 2.4 m s^{-1}, exactly the speed of the background wind at the height of the inflection point. The horizontal wavelength is 262 m, or 6.55 Δz, which is comparable with the values of 4.4 Δz and 7.5 Δz suggested by Drazin (1958) and Miles and Howard (1964), respectively. The growth rate of the disturbance is about 0.0125 s^{-1}, implying an e-folding time of a little more than 8 min. The K-H perturbations, therefore, grow quickly enough to become physically important.

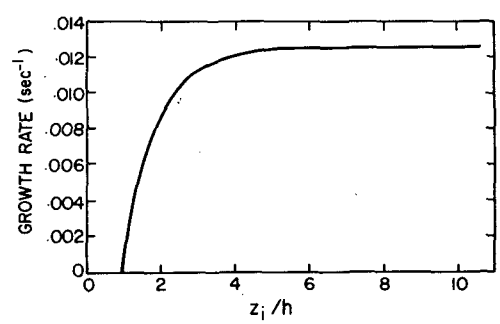

FIG. 4. Growth rate of the fastest growing K-H mode as a function of z_i/h: $h=20$ m, $\alpha=0.8$ K, $\beta=1$.

Fig. 5a shows the normalized eigenfunctions of the fastest growing K-H disturbance for $z_i/h=30$. Here the eigenfunction is represented by the magnitude $|w|$ of the vertical velocity perturbation. The amplitude of the disturbance both above and below the shear layer is attenuated by a factor e within 44 m. Since the vertical wavelength of the disturbance away from the shear layer is about 12 km, the attenuation is certainly complete long before the disturbance can undergo a single oscillation.

These characteristics are considerably modified once the effect of the wall is felt. The phase speed of the disturbance drops below 2.4 m s^{-1}. The horizontal wavelength increases and then decreases in response to the introduction of the new length scale z_i. The perturbation is still strongly attenuated above and below the shear layer, but the presence of the wall induces an asymmetry in the eigenfunctions (Fig. 5b).

The following calculations involve the behavior of the K-H modes with β, R_h and R_α. They were made for $z_i/h=15$, so that the fastest growing modes are essentially unaffected by the presence of the ground.

Fig. 6 shows the variation in the horizontal wave-

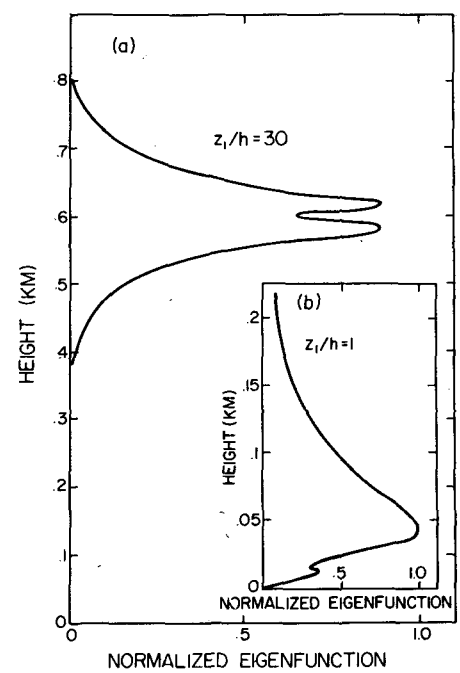

FIG. 5. Normalized eigenfunctions of the fastest growing K-H mode at $z_i/h=30$ (a) and $z_i/h=1$ (b). The height of the inflection point is 0.6 km in (a), and 0.02 km in (b). The critical level occurs at the height of the minimum in the eigenfunction in each case.

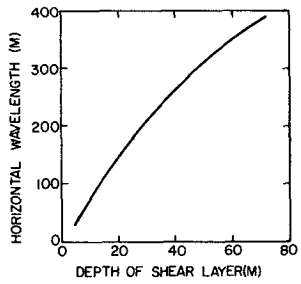

FIG. 6. Horizontal wavelength of the fastest growing K-H mode as a function of shear depth: $z_i/h=15$, $\alpha=0.8$ K, $\beta=1$.

length λ of the fastest growing K-H mode with the shear depth Δz. The relationship is approximately linear, verifying that Δz is indeed the scale which determines the horizontal wavelength of a K-H instability generated well above the ground. We find on the average that

$$\lambda/\Delta z \approx 6.55. \tag{16}$$

This ratio decreases by about 20% as Δz increases from 10 to 65 m. The proportionality between the parameters of the fastest growing mode and the shear depth implies that there is one size of K-H disturbance, measured relative to the depth of the shear layer, that is most efficient in smoothing the shear.

The variation of the growth rate of the fastest growing K-H mode with R_h is shown in Fig. 7a. No instabilities were found beyond $R_h=0.25$, as predicted by theory. The rapid increase in growth rate for small R_h is due to the fact that R_h decreases as the shear increases. The condition $R_h=0$ requires an infinite shear, and an infinitely large growth rate to remove that shear.

Fig. 7b shows the dependence of the K-H growth rates with R_α. Again, no instabilities were found for $R>0.25$. Decreasing stability leads to larger growth rates, as might be expected for disturbances that are not wavelike. The growth rates as functions of β are shown in Fig. 7c. A wide shear zone containing a sharp, narrow temperature increase produces a faster growing disturbance than does a narrow zone of shear embedded in a broader inversion.

In order to demonstrate the applicability of these results to real atmospheric phenomena, we will compare them to a wave generation event observed by Hooke *et al.* (1973). The disturbance was recorded on an acoustic sounder and simultaneously on a microbarograph array, during a period when strong shear coincided with inversion conditions at about 125 m. The sounder record showed a braided pattern between 80 and 150 m that is typical of a K-H disturbance. The depth of the shear layer was observed to be about 50 m, so that in our terminology $z_i/h\approx 5$. Fig. 4 shows that at this height the fastest growing mode is essentially unaffected by the ground, and should have a phase speed equal to the background wind speed at the center of the shear layer. In fact, the observed

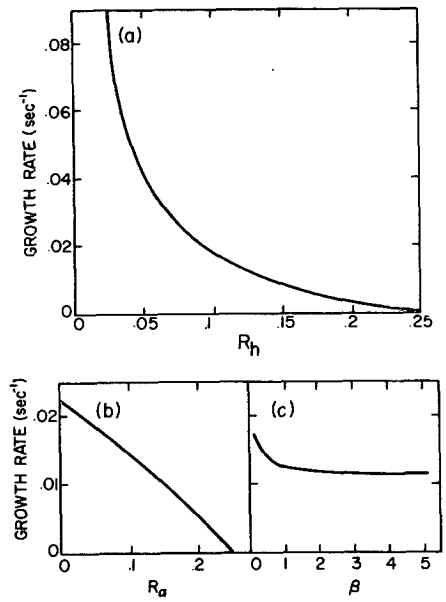

FIG. 7. Growth rate of the fastest growing K-H mode at $z_i/h=15$ as a function (a) of R_h ($\alpha=0.8$ K, $\beta=1$), (b) of R_α ($h=20$ m, $\beta=1$), and (c) of β ($h=20$ m, $\alpha=0.8$ K).

phase speed of the wave was about 3.5 m s^{-1}, while the background wind speed increased from 2.5 to 5 m s^{-1} over the depth of the shear. Fig. 6 indicates that a shear depth of 50 m corresponds to a horizontal wavelength of about 310 m. This value and the 3.5 m s^{-1} wind speed imply a period of 71 s. These results are to be compared with observed values of 350 m and 100 s for

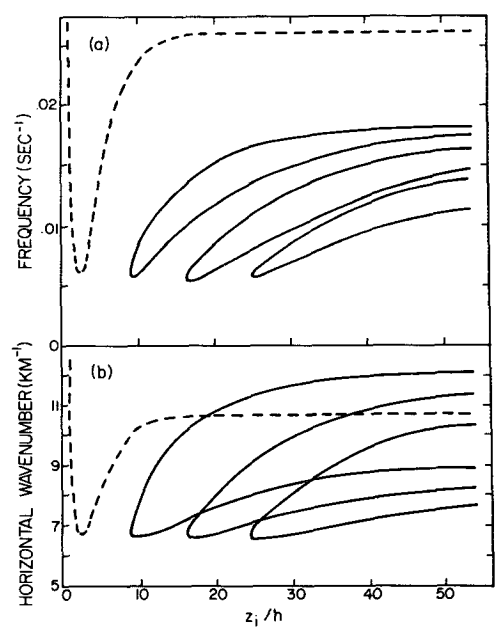

FIG. 8. Frequency (a) and horizontal wavenumber (b) of the first three neutral secondary modes as functions of z_i/h. The lower branch of the K-H neutral curves are shown as dotted lines. ($h=20$ m, $\alpha=0.8$ K, $\beta=1$.)

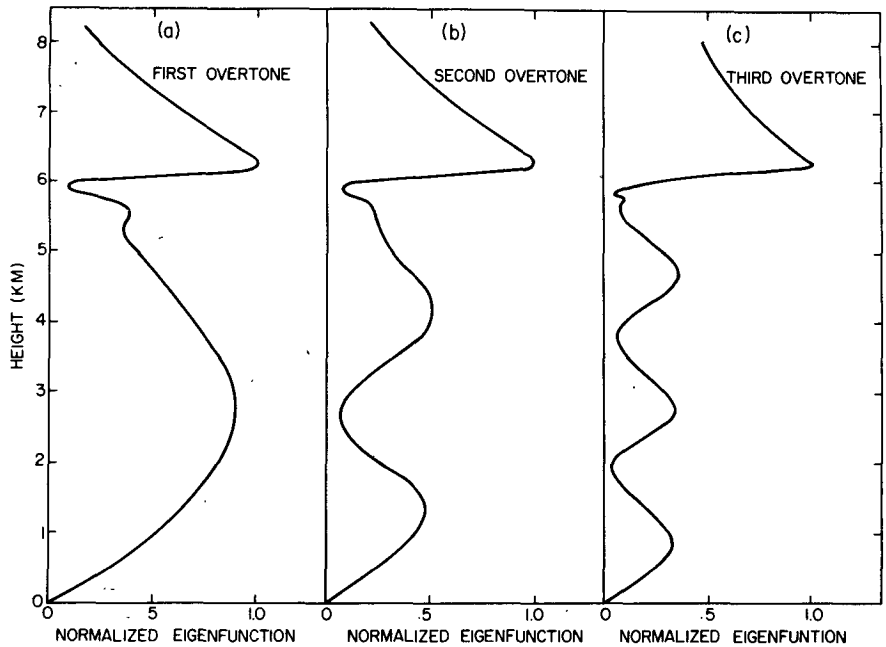

FIG. 9. Normalized eigenfunctions of the fastest growing secondary modes at $z_i/h=30$. The first overtone is shown in (a), the second in (b) and the third in (c). The height of the inflection point is 0.6 km, and the critical level in each case is at the height of the minimum in the eigenfunction. ($h=20$ m, $\alpha=0.8$ K, $\beta=1$.)

the wavelength and period, respectively. This is good agreement considering the fact that the wind speed and temperature profiles were approximated here by hyperbolic tangents, and the fact that the wave was certainly nonlinear in character at the time of observation. In addition, the amplitude of the pressure fluctuations observed at the ground was much less than that observed at 150 m. The wave is therefore strongly attenuated in the vertical, as predicted by theory.

b. Resonant modes: Trapped modes

A further search for neutral eigenvalues at various values of z_i/h (and for the standard values of the other parameters) revealed a series of solutions lying below the K-H neutral curves of Fig. 2. The neutral curves for the first three of these secondary, or overtone, modes are shown in Fig. 8. (We shall denote the secondary mode with the highest frequencies as the first secondary mode, and so on.) Within each overtone mode, no instabilities are found below a minimum, or cutoff, value of z_i/h. In addition, for a given value of z_i/h, the two neutral solutions for each overtone are bounds for growing solutions. These similarities between the secondary modes and the K-H disturbances suggest that all the modes are members of a single family.

Fig. 8 shows that the secondary modes have longer wavelengths and longer periods than the K-H modes. The phase speeds of the secondary modes are all less than 2.4 m s^{-1}, so that the critical levels for these modes are located below the height of the inflection point in the wind profile. The range of possible unstable wavelengths at a given value of z_i/h is small.

The nature of these secondary modes is best understood by examining their eigenfunction structure. Normalized eigenfunctions of the fastest growing modes of the first three secondary disturbances are shown in Fig. 9 for $z_i/h=30$. (The eigenfunctions show much the same structure at all values of z_i/h.) Above the shear layer the eigenfunction amplitude decays fairly rapidly, as was the case for the K-H modes, and the structure at the critical level is similar. Below the shear layer, however, the secondary mode structure is unique. The eigenfunction of the first secondary mode shows a single maximum between the bottom of the shear zone and the ground. The second and third overtones show two and three maxima, respectively, in this layer, and within each mode the amplitudes of the maxima decrease very little away from the shear zone. This lack of attenuation implies that the secondary disturbances can propagate down to the ground, reflect, and return to the shear layer. In so doing, the upgoing and downgoing waves interfer to produce the standing wave pattern of Fig. 9.

This picture is reinforced by the calculation of the vertical wavelengths of the first three secondary modes in the isothermal, wind-free layer between the bottom of the shear zone and the ground. These values are listed in Table 1. The ratio of the isothermal layer depth (about 560 m) to real vertical wavelength is very close to $\frac{1}{2}$, 1 and $\frac{3}{2}$ for the first, second and third

TABLE 1. Real and imaginary vertical wavelengths in the isothermal, wind-free layer between the bottom of the shear zone and the ground ($z_i/h=30$).

Mode	Real vertical wavelength (km)	Imaginary vertical wavelength (km)
1st overtone	1.08	8.6
2nd overtone	0.561	8.24
3rd overtone	0.377	14.5
K-H	11.7	0.276

overtones, respectively. Thus, the allowed secondary modes are those which can fit an integral number of half-wavelengths into the layer between the shear zone and the ground. This selectivity implies a resonant effect, and the secondary modes will in the future be termed resonant modes. In Section 4, the nature of the resonance will be discussed and interpreted in terms of over-reflection (Jones, 1968).

The growth rates of the resonant modes are shown as functions of z_i/h in Fig. 10. As z_i/h increases, there exist successive intervals over which the various overtones in turn have the largest growth rate. The height of the shear layer above the ground therefore determines which member of the resonant family is most likely to become physically important.

We have seen in Fig. 8 that, for a given value of z_i/h, the range of wavenumbers and frequencies available to unstable resonant modes is very much smaller than the corresponding range available to the K-H modes. This fact can be understood by noting that many of the parameters of the resonant modes become fixed once the distance of the shear layer from the wall has been specified. The depth of the isothermal, wind-free layer between the bottom of the shear zone and the ground is given approximately by

$$L=z_i-\Delta z. \tag{17}$$

Into this distance we must fit $n/2$ vertical wavelengths ζ_r, the value of n depending upon the specific overtone. Thus, given z_i and the particular overtone, l_r is fixed. Since l_i is small in this layer, (11) implies that k is approximately proportional to l_r; thus k is also fixed. The value of ω_r is then limited by the requirement that there exist a critical level for the wave somewhere in the flow.

The maximum growth rates for the first three resonant modes are found from Fig. 10 to occur at $z_i/h=19$, 35 and 51, respectively. From (17), the corresponding depths of the isothermal, wind-free layers are 340, 660 and 980 m. These depths are, to a good approximation, in the ratio 1:2:3. This implies that there is a single vertical wavelength which leads to a maximum growth rate for all resonant modes. This, in turn, indicates that the vertical wavelength which will most efficiently smooth a shear layer of depth Δz is given by

$$\zeta_r=16.5\,\Delta z. \tag{18}$$

Note that the numerical factor in (18) applies to the specific background configuration defined by $h=20$ m, $\alpha=0.8$ K and $\beta=1$, and will vary by up to 20% for different background profiles.

Condition (18) is reminiscent of Eq. (16), which gave the horizontal wavelength of the K-H mode which was most efficient at smoothing a given shear layer. However, the two equations must be interpreted differently. Eq. (16) implies that, given a shear layer of depth Δz, there exist among the possible K-H disturbances a particular mode with a wavelength which will smooth the shear layer fastest. On the other hand, (18) states that, for a given Δz, there exists an optimum resonant vertical wavelength for extracting energy, but this wavelength will be realizable only if the shear layer is located at a particular distance from the wall. Using the relation $L\approx n\zeta_r/2$, the maximum growth rate for the overtone of order n will occur when $L/\Delta z\approx 8.25n$.

We note from Fig. 10 that the values of z_i/h at which the growth rates of the first three resonant modes drop to zero are 8.8, 16.1 and 24.4, respectively. These values again lead to isothermal, wind-free layer depths in the ratio 1:2:3. Therefore, no resonant instabilities are possible if $\zeta_r<7\ \Delta z$, or if $L/\Delta z<3.5\ n$. Again the numerical values given here should be applied with caution.

An interesting feature of the neutral solutions corresponding to resonant modes is seen in Fig. 11, where the frequencies of the first three resonant modes are plotted against their corresponding horizontal wavenumbers for all values of z_i/h. The points fall naturally onto two straight lines which tend to curve toward each other at small values of ω_r and k. The upper line is formed of points from the lower branches of the neutral curves of Fig. 8, and the lower line of points from the upper branches. The points connecting the two lines are points from the areas of Fig. 8 where the neutral curves turn back on themselves. Each of these

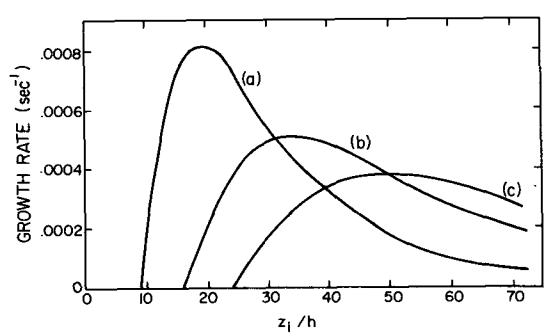

FIG. 10. Growth rates of the resonant modes as functions of z_i/h. Curves (a), (b) and (c) correspond to the first, second and third overtone respectively. ($h=20$ m, $\alpha=0.8$ K, $\beta=1$.)

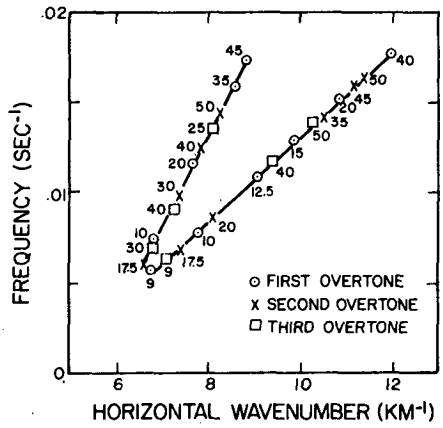

FIG. 11. Frequency as a function of horizontal wavenumber for the neutral resonant modes. The points are taken from Fig. 8 and plotted without regard to the order of the overtone or the value of z_i/h. The number beside each point is the value of z_i/h appropriate to that point. ($h=20$ m, $\alpha=0.8$ K, $\beta=1$.)

lines has an equation of the form

$$\omega_r - sk = b, \tag{19}$$

where s is the slope of the line and b its intercept on the k axis. But (19) is simply a statement that the Doppler-shifted frequency of a wave with frequency ω_r in a fixed frame and with wavenumber k is a constant b at a level where the wind speed is s. The least square values of s for the upper and lower lines respectively are 2.41 and 4.95 m s^{-1}. These values are sufficiently close to 2.40 and 4.80 to conclude that all neutral resonant solutions, regardless of their particular family membership or of the distance of the shear layer from the wall, have one of two Doppler-shifted frequencies, the frequency relevant either at the inflection point height, or in the upper half-space.

The growth rates of the various resonant modes shown in Fig. 10 are all small, and in particular are smaller than the K-H growth rates by a factor of 15 or more. However, it was found possible to improve the resonant growth rates, in both an absolute and relative sense, by varying the values of the background parameters. The variation of the growth rates of the resonant modes with β, R_h and R_α are shown in Figs. 12, 13 and 14, respectively. These calculations were pursued only for the first resonant mode for $z_i/h=19$, where the growth rate of this overtone is maximized. Both the absolute resonant growth rates and the ratio of resonant to K-H growth rates are shown in these figures.

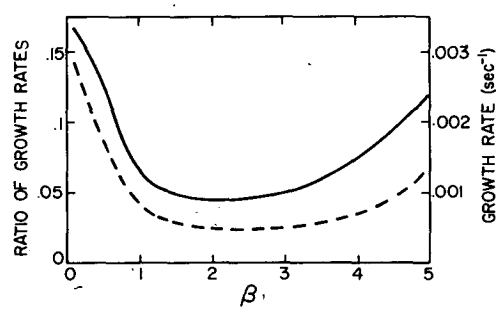

FIG. 12. Growth rate of the first resonant mode as a function of β. The ordinate on the left applies to the solid curves while the ordinate on the right applies to the dashed curve. ($z_i/h=19$, $h=20$ m, $\alpha=0.8$ K.)

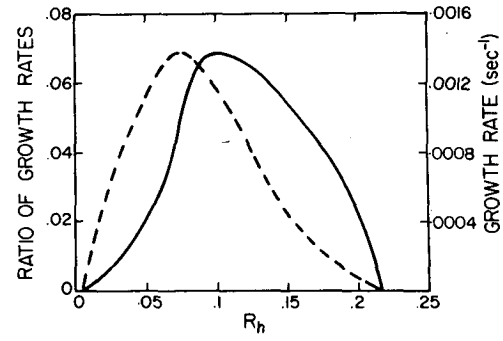

FIG. 13. As in Fig. 12 except as a function of R_h. ($z_i/h=19$, $\alpha=0.8$ K, $\beta=1$.)

Fig. 12 shows that the resonant growth rates are enhanced, in both the absolute and the relative sense, whenever the scale of the temperature gradient is markedly different from the scale of the shear. In Fig. 13, the absolute resonant growth rates are seen to increase as R_h is decreased to 0.075, but the rapid increase in the K-H growth rates at small R_h means that the relative rates decrease for $R_h<0.10$.

Fig. 14 illustrates that decreased static stability leads to generally higher resonant growth rates. This is perhaps surprising in that the bouyant restoring forces necessary for wave motion weaken as the stability decreases.

Figs. 13 and 14 demonstrate that R must be significantly less than 0.25 before resonant instabilities appear. On the other hand, K-H disturbances are found immediately as R drops below 0.25. Thus, the Miles-Howard criterion appears to be a sufficient condition for K-H instability, but only a necessary condition for resonant instability. This is in accord with the interpretation of the resonant modes in terms of over-reflection.

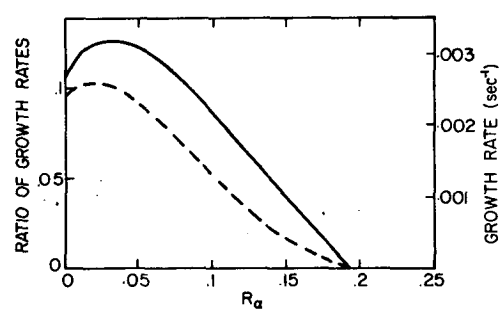

FIG. 14. As in Fig. 12 except as a function of R_α. ($z_i/h=19$, $h=60$ m, $\beta=1$.)

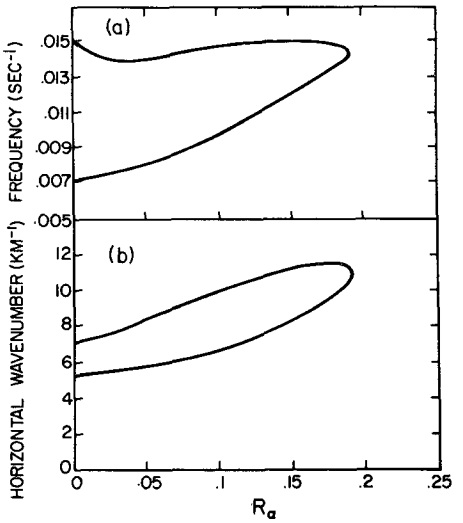

FIG. 15. Frequency (a) and horizontal wavenumber (b) of the first neutral resonant mode as functions of R_α: $z_i/h=19$, $h=20$ m, $\beta=1$.

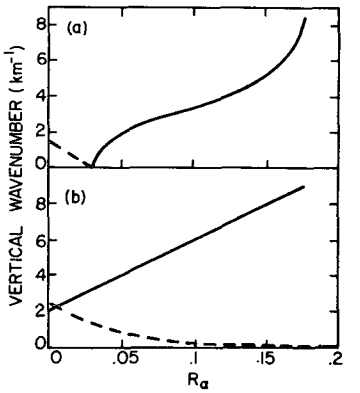

FIG. 16. Real (dashed curve) and imaginary (solid curve) vertical wavenumbers in the lower isothermal, wind-free layer as functions of R_α. The wavenumbers of the neutral modes lying in the lower branch of Fig. 15 are shown in (a). The wavenumbers of the fastest growing modes related to the neutral curves of Fig. 15 are shown in (b). ($z_i/h=19$, $h=20$, $\beta=1$.)

The largest growth rates in any of Figs. 12–14 occur for small values of β and R_α, and correspond to e-folding times of a little less than 40 min. This value could no doubt be improved by considering a model in which both β and R_α were small. These growth rates are sufficiently large that the resonant modes could become physically important if the shear layer which was responsible for their generation was maintained for a period of 2 or 3 h.

c. *Resonant modes: Propagating modes*

Almost all of the resonant modes discussed in the previous section were strongly attenuated in the isothermal, constant-wind region above the shear layer. Exceptions to this rule are the modes generated by the almost isentropic shear layers which obtain at small R_α. The neutral eigenvalues for these modes are shown in Fig. 15. The real and imaginary parts of the vertical wavenumbers of the modes lying in the lower branch of these curves appear in Fig. 16a. For large values of R_α, the disturbance is evanescent in the upper half-space, as l_r is zero here and l_i non-zero. However, for $R_\alpha<0.03$ the situation is reversed, and the modes become free to propagate without attenuation in the upper half-space.

The same behavior can be seen in Fig. 16b in the growing modes. At large values of R_α, the rate of attenuation in the upper half-space is so high that the disturbance is extinguished long before it can undergo a single oscillation. However, as R_α decreases both the vertical wavelength and the attenuation decrease until, at $R_\alpha=0.005$, the wave can propagate over a full wavelength before it is attenuated by a factor e. Since the wavelength at this point is about 2.5 km, the wave can carry energy and momentum to considerable heights above the shear zone.

The value of R_α at which neutral modes become propagating modes also appears to mark a change in the relationship between the neutral and growing solutions. For a given value of R_α greater than 0.03, the two neutral solutions are bounds for growing modes, and the stability curve looks much like that of Fig. 3. However, for $R_\alpha<0.03$, the lower branch of the neutral curve ceases to be the stability boundary for growing modes. The stability curve for $R_\alpha=0.025$ is shown in Fig. 17. The growing solutions no longer evolve into the lower neutral solution, but are found on either side of the neutral curve. In particular, the growing solutions outside the neutral curve extend to very small values of frequency and wavenumber, so that

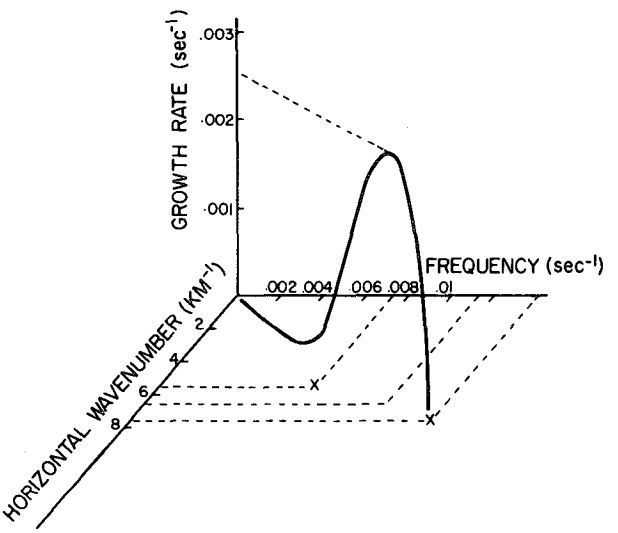

FIG. 17. As in Fig. 3 except at $R_\alpha=0.025$. ($z_i/h=19$, $h=20$ m, $\alpha=0$, $\beta=1$.)

the range of possible periods and wavelengths for instability is vastly increased. The simultaneous appearance of propagating solutions and non-contiguous growing modes suggests that these two features might always appear together.

It is possible that the non-contiguous growing solutions are in fact bounded by a neutral curve which branches off from the neutral curve shown in Fig. 15. The situation would then be similar to that shown in Fig. 1 of Blumen *et al.* (1975) for the case of supersonic instabilities of a shear layer embedded in an inviscid, compressible fluid free from gravitational stratification. This figure shows that growing solutions extend over one branch of the associated neutral curve, but are bounded by a second branch of the same curve. In the present case, a detailed search near $R_\alpha=0.03$, where such a splitting would most obviously occur, failed to reveal a secondary branch. We have not looked in any detail for a branching at larger values of R_α.

The non-contiguous modes found in the present study imply that theorem IV of Section 2 cannot be extended to the flows considered here. The close relationship between the neutral and growing solutions implied by this theorem is broken by the present asymmetry in the boundary conditions.

4. Discussion and conclusions

We have shown in the previous sections that the introduction of a rigid boundary below a stratified parallel shear flow leads to modes of instability other than the well-known K-H disturbance. We were able to define the frequencies, wavelengths and growth rates of these modes as functions of the parameters of the background flow, and to deduce their behavior above and below the region of shear. However, there remain a number of questions which cannot be answered in the framework of linear theory. These will be discussed qualitatively below. A quantitative analysis will have to await the solution of the associated initial value problem. This is a subject of current study.

The first question concerns the nature of the resonance which is responsible for the existence and structure of the resonant modes. Since the conditions under which the initial generation of the instability occurs are similar to those studied by Lindzen (1974) we expect the original perturbation to appear as a neutral wave. This wave propagates downward and reflects from the ground, and must interact in some manner with its critical level when it returns to the shear layer. The most likely form of such interaction is over-reflection (Jones, 1968), the physical manifestation of which is seen in the non-zero growth rates of the resonant modes. The ground is therefore responsible, not for the existence of the wavelike modes, but for the non-zero values of their growth rates, as was conjectured by Lindzen (1974). The ground is also certainly responsible for the standing wave pattern of their eigenfunctions.

In the case of the nearly isentropic shear layer, in which the perturbation radiates upward from the shear zone as well as downward, there are two possibilities. The upward wave may be emitted at the moment of generation of the instability, or the wave reflected from the ground may be partially transmitted on its return to the critical level. In the latter case, the weakened resonant interaction at the critical level may explain the falloff in growth rate at small R_α observed in Fig. 14.

A second question involves the mechanism by which the trapped resonant modes may serve to smooth the background shear. In the usual case of propagating disturbances, excess energy in the mean flow is used to generate the wave, which then carries this energy far from the region of shear to deposit it wherever the wave is re-absorbed by the mean flow. However, in the case of the resonant modes, the energy and momentum carried away from the shear layer by the downgoing wave are continuously distributed in the growing standing wave. When this standing wave breaks the attendant redistribution of momentum may be highly anisotropic. We have shown in the previous section that the resonant modes do in fact grow slowly so that given sufficient time the boundary layer momentum profile will be significantly modified by their existence.

A simplified picture of the breakdown process itself may be as follows. Between the bottom of the shear layer and the ground, the vertical structure of the perturbation horizontal velocity is much the same as that of the perturbation vertical velocity as shown in Fig. 9, except that levels where maxima in $|w'|$ occur are now levels where minima in $|u'|$ occur, and vice versa. The largest shears in this region will therefore exist at heights halfway between these maxima and minima. As the waves grow these shears may become large enough to force the Richardson number below 0.25, and small-scale K-H disturbances will develop. These disturbances will in turn grow and break, resulting in thin bands of turbulence along the nodal lines. Because of the symmetry in the eigenfunction pattern, these turbulent layers will be coherent and equally spaced in the vertical.

The similarity between these conclusions and the radar records suggests that resonant modes are responsible for the formation of the multiple thin layers commonly observed in the boundary layer. Unfortunately, to the authors' knowledge there have been no studies published in which both atmospheric soundings and measurements of the wave parameters have accompanied radar observations of multiple layer events. The results obtained above cannot, therefore, be compared quantitatively with specific observations. However, qualitative agreement is found with at least one feature of the results of Beran *et al.* (1973) who obtained wave parameters from microbarograph observa-

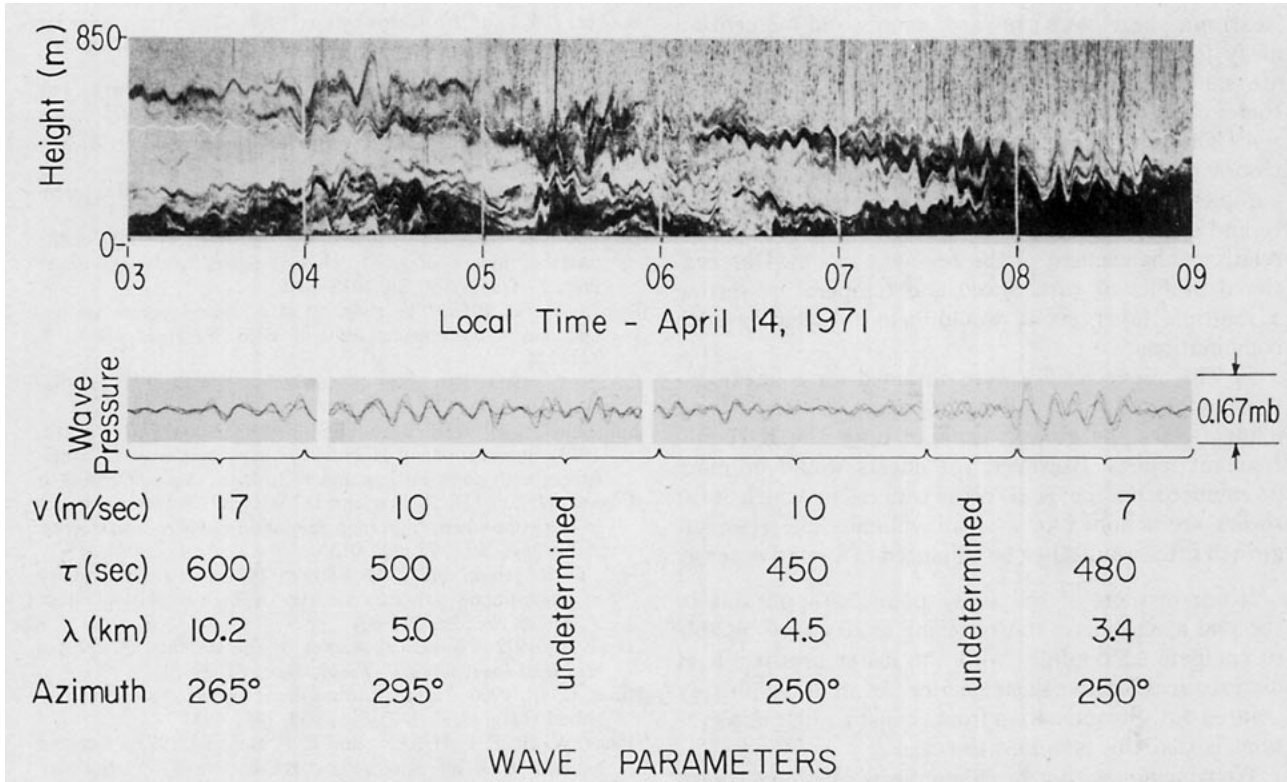

FIG. 18. Sounder record (Fig. 8 of Beran *et al.*, 1973) showing several examples of multiple thin wavy layers. The white line superimposed on the record is the pressure trace from a microbarograph located roughly 800 m from the sounder. The wave parameters deduced from the microbarograph observations are indicated in Table 1.

tions during a series of multiple layer events. Fig. 18 is a reproduction of Fig. 8 of Beran *et al.*, and shows the microbarograph and sounder records of interest. We will assume, in the absence of actual soundings, that the disturbed region in Fig. 18 is capped by an inversion with embedded shear. According to the present model the vertical wavelength of a given overtone should decrease as the depth of the disturbed layer decreases. Eq. (11) then predicts that the horizontal wavelength will also decrease. The observations show, in fact, that a decrease in the depth of the disturbed layer in time is accompanied by a decrease in the horizontal wavelength of the observed waves.

The final point to be discussed concerns the possible ways in which the disturbance field might evolve when the two modes of instability, K-H and resonant, compete for the energy available in the mean flow. At first glance it would seem that the K-H modes would grow so quickly that they would smooth the background shear before the resonant modes could be significantly amplified. However, the problem is more subtle than this and several additional factors need to be considered.

1) Most multiple layer events are observed in marine (Gossard *et al.*, 1971) or arctic (Beran *et al.*, 1973, Fig. 3) inversions, both of which are maintained by radiative effects and are therefore quite persistent. The multiple layers themselves are fairly long-lived events, often lasting for an hour or more. Both of these points suggest that the time required for the resonant modes to grow to maturity is in fact available to them.

2) The breakdown of the resonant modes may be accelerated by the formation of large gradients in the perturbation velocity in a process similar to that described by Teitelbaum and Sidi (1975). These researchers studied gravity wave propagation in the upper atmosphere over distances large enough that the vertical decrease in density led to significant increases in the wave amplitude. They found that discontinuities in the wave field appeared quickly whenever two or more such waves interacted. In the boundary layer, the growth of wave amplitude with height would be replaced by the growth in time which the resonant modes have been shown to undergo. Even though this growth takes place relatively slowly, the interaction between the upgoing and downgoing waves reduces the time required for discontinuities in the wave fields to occur. The horizontal discontinuities in velocity thus produced will quickly enhance the large shears which already exist at the nodal points of the standing waves, and breakdown will follow rapidly. Observational evidence that the interaction between an upgoing and a downgoing wave can lead to enhanced instability is found in Fig. 18 of Gossard *et al.* (1971).

3) The propagating resonant modes generated by

isentropic shear flows can carry energy and momentum away from the shear zone even if their growth rates are small. The true importance of these modes may therefore be underestimated by their small growth rates.

4) The growth rates of both the K-H and resonant modes were found to vary considerably with the parameters of the background flow. It may be possible to find combinations of the parameters which lead to a relative enhancement of the resonant modes. Observational profiles of wind speed and temperature during a multiple layer event would help to identify such combinations.

5) The above results were obtained for a linear, inviscid model. In the real atmosphere, viscosity would likely reduce the growth rates of both the K-H and resonant modes. However, the effects would be more pronounced on the K-H disturbances, in which large shears are confined to a small volume. The resonant growth rates would then be enhanced in a relative sense.

If one or more of the above points is applicable to the real atmosphere, the resonant modes may be able to compete successfully with the faster growing K-H disturbances for the shear energy. As we have already pointed out, the indication from acoustic radar observations is that this is indeed the case.

We conclude with a brief summary. We have shown that a parallel shear flow above a rigid boundary is unstable to perturbations which have the character of internal gravity waves. In cases of strong static stability these disturbances are trapped between their critical level and the ground. The eigenfunction structure of these modes suggests an explanation for the multiple thin wavy scattering layers commonly observed in the stable boundary layer. For nearly isentropic shear layers, the resonant modes are no longer trapped, but are able to carry energy and momentum to considerable distances above the shear zone. We are presently attempting to answer questions concerning the nonlinear development of these waves by solving the associated initial value problem.

REFERENCES

Bennett, R. C., 1975: Acoustic radar studies of planetary boundary layer structures associated with gravity waves, fronts and lake breezes. Ph.D. thesis, University of Toronto, 308 pp.

Beran, D. W., W. H. Hooke and S. F. Clifford, 1973: Acoustic echo-sounding techniques and their application to gravity wave, turbulence and stability studies. *Boundary-Layer Meteor.*, **4**, 133–153.

Blumen, W., P. G. Drazin and D. F. Billings, 1975: Shear layer instability of an inviscid compressible fluid. Part 2. *J. Fluid Mech.*, **71**, 305–316.

Booker, J. R., and F. P. Bretherton, 1967: The critical layer for internal gravity waves in a shear flow. *J. Fluid Mech.*, **27**, 513–539.

Browning, K. A., J. R. Starr and A. J. Whyman, 1973: The structure of an inversion above a convective boundary layer as observed using high power pulsed Doppler radar. *Boundary-Layer Meteor.*, **4**, 91–111.

Chimonas, G., 1970: The extension of the Miles-Howard theorem to compressible fluids. *J. Fluid Mech.*, **43**, 833–836.

Dickinson, R. E., and F. J. Clare, 1973: Numerical study of the unstable modes of a hyperbolic-tangent barotropic shear flow. *J. Atmos. Sci.*, **30**, 1035–1049.

Drazin, P. G., 1958: The stability of a shear layer in an unbounded heterogeneous inviscid fluid. *J. Fluid Mech.*, **4**, 211–224.

Eckart, C., 1963: Extension of Howard's circle theorem to adiabatic jets. *Phys. Fluids*, **6**, 1042–1047.

Emmanuel, C. B., B. R. Bean, L. G. McAllister and J. R. Pollard, 1972: Observations of Helmholtz waves in the lower atmosphere with an acoustic sounder. *J. Atmos. Sci.*, **29**, 886–892.

Gossard, E. E., J. H. Richter and D. Atlas, 1970: Internal waves in the atmosphere from high-resolution radar measurements. *J. Geophys. Res.*, **75**, 903–913.

——, D. R. Jensen and J. H. Richter, 1971: An analytic study of tropospheric structure as seen by high-resolution radar. *J. Atmos. Sci.*, **28**, 794–807.

Hazel, P., 1972: Numerical studies of the stability of inviscid stratified shear flows. *J. Fluid Mech.*, **51**, 39–61.

Hines, C. O., 1960: Internal atmospheric gravity waves at ionospheric heights. *Can. J. Phys.*, **38**, 1441–1481.

Hooke, W. H., F. F. Hall, Jr., and E. E. Gossard, 1973: Observed generation of an atmospheric gravity wave by shear instability in the mean flow of the planetary boundary layer. *Boundary-Layer Meteor.*, **5**, 29–42.

Howard, L. N., 1961: Note on a paper of John W. Miles. *J. Fluid Mech.*, **10**, 509–512.

Jones, W. L., 1968: Reflexion and stability of waves in stably stratified fluids with shear flow: A numerical study. *J. Fluid Mech.*, **34**, 609–624.

Kaylor, R., and A. J. Faller, 1972: Instability of the stratified Ekman boundary layer and the generation of internal waves. *J. Atmos. Sci.*, **29**, 497–509.

Lindzen, R. S., 1974: Stability of a Helmholtz velocity profile in a continuously stratified, infinite Boussinesq fluid—applications to clear air turbulence. *J. Atmos. Sci.*, **31**, 1507–1514.

Metcalf, J. I., 1975: Gravity waves in a low-level inversion. *J. Atmos. Sci.*, **32**, 351–361.

Miles, J. W., 1961: On the stability of heterogeneous shear flows. *J. Fluid Mech.*, **10**, 496–508.

——, 1963: On the stability of heterogeneous shear flows. Part 2. *J. Fluid Mech.*, **16**, 209–227.

——, and L. N. Howard, 1964: Note on a heterogeneous shear flow. *J. Fluid Mech.*, **20**, 311–313.

Orlanski, I., 1973: Trapeze instability as a source of internal gravity waves. Part I. *J. Atmos. Sci.*, **30**, 1007–1016.

Teitelbaum, H., and C. Sidi, 1975: Formation of discontinuities in atmospheric gravity waves. *J. Atmos. Terr. Phys.* (in press).

Yih, C. S., 1955: Stability of two-dimensional parallel flows to three-dimensional disturbances. *Quart. Appl. Math.*, **12**, 434–435.